FEM ANALYSIS OF ANTI-MINING PROTECTION OF ARMORED VEHICLES

UDC:519.61:623.438
Original scientific paper https://doi.org/10.18485/aeletters.2022.7.3.1

Miloš Pešić[1*], Nikola Jović[2], Vladimir Milovanović[2], Danilo Savić[3], Aleksa Aničić[4], Miroslav Živković[2], Slobodan Savić[2]

[1] University of Kragujevac, Institute for Information Technologies – National Institute of the Republic of Serbia, Jovana Cvijica bb, 34000 Kragujevac, Serbia
[2] University of Kragujevac, Faculty of Engineering, Sestre Janjić 6, 34000 Kragujevac, Serbia
[3] Data Cloud Technology DOO, Save Kovacevica 35b, 34000 Kragujevac, Serbia
[4] Agency for Testing, Stamping and Marking of Weapons, Devices and Ammunition, Stojana Protica bb, 34000 Kragujevac, Serbia

Abstract:
The safety of the troop in an armored vehicle is paramount. The most serious threat to armored vehicles is a buried charge explosion or an improvised explosive device. The use of numerical approaches in the validation of armored vehicles minimizes the number of prototypes needed and speeds up the design process. This research focuses on blast simulation utilizing the ConWep (which stands for conventional weapon) method for STRENX armor steel used for blast protection in ALM (which stands for anti-landmine) vehicles. The plate is modeled as a deformable solid with the Johnson-Cook plasticity model. In this paper protective plates were examined in order to determine which geometry gives the best protective conditions for the troop in an armored vehicle. Three different geometries were numerically tested, and two of them represent combined geometry. The maximal value of the plastic strain and maximal value of the vertical displacement of the central node on the protective plate was chosen as the parameters to represent the obtained results.

ARTICLE HISTORY
Received: 12.07.2022.
Accepted: 13.09.2022.
Available: 30.09.2022.

KEYWORDS
Anti-mining protection, blast loading, explicit dynamics, finite element method

1. INTRODUCTION

When an air blast interacts with structures, it creates a pressure wave that deforms them and renders them useless. In order to reduce the deformation of the vehicle [1], and thus increase the safety of the troop in the armored vehicle, it is necessary to examine the impact of the blast wave on the vehicle and its systems. One of the most important systems on the vehicle is a braking system. Its main task is to maintain vehicle speed and adapt to road conditions [2]. The paper [3] represents a validation of the use of numerical methods in the designing process of armored vehicles because it reduces the number of prototypes required and decreases the design time.

Ballistic materials are used to prevent excessive deformations in constructions and vehicles. Steel is the most common material used to protect against anti-mining. In paper [4], the influence of the blast wave of an explosion on laminated and monolithic plates was investigated. Material characteristics of STRENX700 steel were used as input data for numerical analysis.

The body of a vehicle is clad with armor steel plates for blast protection, making it an armored vehicle. Explosion protection plates can be of different geometries. Some of the geometries used are V-shape [5-7], and flat shape [4,5,8]. The paper [5] presents the comparisons of the results for armored vehicles with a flat hull floor and its modified V-hull floor version. For FE models creating Smooth Particle Hydrodynamics - Finite Element (SPH-FE) combination was used.

Depending on the protective plate geometry of the armored vehicle, the troop suffers different

*CONTACT: M. Pešić, e-mail: milospesic@uni.kg.ac.rs

levels of injuries. Different V-hull shapes were used to investigate the level of force on the troop [6].

In order for the armored vehicle to suffer as little damage as possible, it is necessary to determine the optimal angle of V-shaped protective plates. The estimation of impulse and deflection within the fracture limits is of paramount importance for troop protection [7]. For the purpose of guiding the clinical care of explosion victims, in paper [9,10] is presented the physics of the vehicle mine blast, the likely pathways of injury to troops, and the development of countermeasures to limit this threat.

Blast-wave dispersion under the armored vehicle with the flat floor anti-mine protection was examined in order to determine the magnitude of the kinetic energy acting on the armored vehicle chassis and the vertical displacement generated by energy [8].

Research in this paper was conducted in accordance with NATO AEP-55 STANAG 4569 standard - levels 3 and 4 [11].

In this paper, the main objective is to determine which geometry of the protective plate on the armored vehicle, based on the obtained numerical results, is the most suitable. The aim is to protect troops and armored vehicles from the blast wave generated by ALM.

2. FINITE ELEMENT FORMULATION

In this paper, an explicit dynamic formulation of the finite element equations of structural dynamics is used. The equations of equilibrium in the current configuration have the following form:

$$M^t\ddot{U} + C^t\dot{U} = {}^tR - {}^tF \qquad (1)$$

where the following symbols represent:

M^t - constant matrix mass at the moment t ,

C^t - damping matrix constant at the moment t ,

$\dot{U}$ - node velocity vector,

$\ddot{U}$ - node acceleration vector,

${}^tR$ - external force vector at the moment t and

${}^tF$ - the nodal force vector at the moment t .

Since the explicit method used by LS-DYNA provides fast solutions for short-time, large deformation dynamics, quasi-static problems with large deformations, multiple non-linearity, and complex contact/impact problems, it is used for this research. The general simulation in this study is done with the arbitrary Lagrangian-Eulerian (ALE) approach, which entails modeling the explosive with the ALE multi-material mesh and modeling reinforced anti-mining steel protection for armored vehicles with the Lagrangian mesh.

3. MATERIALS AND METHODS

Various materials are used as blast-resistant materials. Different types of steel [4, 12-15], composite materials [16,17], foams [18], and concrete [19] are among the most commonly utilized materials. The level of protection and weight of each of these materials varies. The weight of these materials is very important since it has a significant impact on vehicle performance.

3.1 Material model

Armor steels are well established as blast-resistant materials. For troops and vehicles protection four different commercial armour steels were experimentally tested in paper [12]. The material suffers plastic flow at high strain rates, temperature increase, and eventual material fracture when the blast wave interacts with the structure. The modified Johnson-Cook material model is the most widely used in the current literature on numerical modeling since it takes strain rate, hardening, and temperature effects into effect. Eq. 2 provides the model equivalent stress. The von Misses tensile flow stress, along with strain hardening, strain rate hardening, and thermal softening, determine the Johnson-Cook material model.

$$\sigma_{eq} = \left[A + B\left(\varepsilon^p\right)^n\right]\left[1 + C\log_e\left(\dot{\varepsilon}^*\right)\right]\left[1 + \left(T^*\right)^m\right] \qquad (2)$$

where:

A, B, C, n, and m are material constants that can be determined by Johnson and Cook's recommended tests (1985). Split Hopkinson Pressure Bar (SHPB) is used as instrumented loading device in dynamic fracture experiments. With SHPB are determined the most of the parameters needed for the Johnson-Cook material model [20]. The first component in Equation 2 denotes the contribution of equivalent stress from the material's strain-rate sensitivity; the second term denotes the effect of strain-rate hardening; and the third term denotes the effect of temperature softening. As specified in Eq. 3, the non-dimensional temperature *(T*)* is the governing term for thermal softening.

$$T^* = (T - T_{ambient})/(T_{melting} - T_{ambient}) \quad (3)$$

Damage initiation in the material is specified by the Johnson and Cook Damage Model using Eq. 4. In Eq. 4, the first parenthesis indicates the strain to fracture, which decreases as hydrostatic stress rises, the second parenthesis indicates the impact of an increasing strain rate on the ductility of the material, and the third parenthesis indicates the impact of thermal softening.

$$\varepsilon_f = \left[D_1 + D_2 e^{D_3 \sigma^*}\right]\left[1 + D_4 \log_e \dot{\varepsilon}^*\right]\left[1 + D_5 T^*\right] \quad (4)$$

where:

$$\sigma^* = \frac{\sigma_m}{\sigma_{eq}} \quad (5)$$

is the stress-triaxiality ratio.

Due to the availability of pertinent information, this study uses the commercially available steel known as STRENX700. Table 1 lists the Johnson-Cook material characteristics for STRENX700. Young's Modulus *(E= 228 GPa)* and Poisson's ratio *(v=0.3)* of STRENX700 Steel is equivalent to mild steel but STRENX700 Steel is much stiffer during loading due to higher strength *(σ_y=750 - 800 MPa).*

Table 1. Johnson-Cook material characteristics for STRENX700

Parameters		Values
Density	*ρ [t/mm³]*	7.85E-9
Young's Modulus	*E [MPa]*	228368.9
Poisson's ratio	*v*	0.33
Yield stress	*A [MPa]*	767.38
Proportionality coefficient	*B [MPa]*	445.13
Reinforcement exponent	*n*	0.5075
Strain rate Impact parameter	*C*	0.0265
Temperature impact parameter	*m*	1.354
Damage parameters	D_1	-0.066
	D_2	3.028
	D_3	-1.408
	D_4	-0.00851
	D_5	0.633

3.2 Finite element model

The significance of the geometric shapes of protective plates in the reduction of incident waves of explosions, i.e. form of additional protection, is analyzed in this paper. Also, when the characteristics of welded joints [21] are taken into consideration, it is possible to analyze much more complex geometric shapes of protective plates that can be considered as a solution for anti-landmine protection. It is also important to note that the clearance value is the same for all analysed models. The mass of TNT explosives corresponds to levels 3 and 4 of protection according to the NATO standard [11] and their mass is 8 kg and 10 kg. In addition, the influence of the mass of the explosive of 12 kg was analyzed. The plate thickness of all models is 10 mm. Based on the CAD model and after creating the FEM model in the FEMAP v2021.2 software [22], the input file for the LS-DYNA software [23] was exported. In LS-DYNA software all other settings and preparations of the FEM model for explicit dynamic analysis were performed. Details of this method implementation and step by step guide for blast load analysis are given in papers [24,25]. Pre-processing and post-processing were performed in the FEMAP v2021.2 software package. All plates were exposed to a hemispherical incident wave. The floor of the vehicle, i.e. the parts of the supporting structure are modelled with 3D hexahedral eight-noded finite elements, while the protective plates are modelled with four-noded plate finite elements. The distance between TNT and a protective plate in all models was 0.5 m. The first FEM model, which represents geometry I – U-shaped geometry for ALM protection, was modelled with 6800 3D hexahedral eight-noded finite elements and 7600 four-noded plate elements and it is shown in Fig. 1.

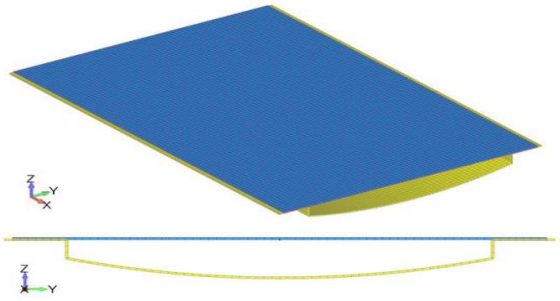

Fig.1. FEM model 1 – Geometry I – U-shaped geometry for ALM protection

The second FEM model, which represents combined geometry II for ALM protection – consists of flat and V-shaped geometry. FEM model 2 was modeled with 6700 3D hexahedral eight nodes finite elements and 7600 four noded plate elements and it is shown in Fig. 2.

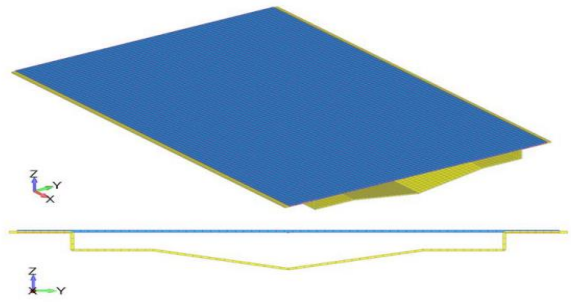

Fig.2. FEM model 2 – combined geometry II for ALM protection

The third FEM model, which represents combined geometry III for ALM protection – consists of V-shaped and flat geometry. FEM model 3 was modeled with 6700 3D hexahedral eight nodes finite elements and 7300 four noded plate elements and it is shown in Fig. 3.

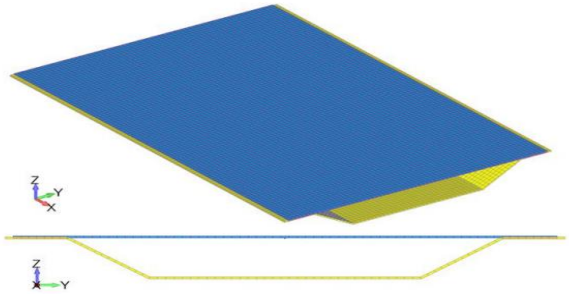

Fig.3. FEM model 3 – combined geometry III for ALM protection

A thin plate responds to loading by bending and stretching its membrane. The lower plate is modeled with four-noded plate elements and the blast loading is applied to it.

Surface-blast produces hemispherical incident waves that propagate across the accessible medium, whereas air-blast generates spherical incident waves. For the purpose of simulating pressure waves caused by the explosion of an explosive for both air and surface blast, LS-DYNA has the ConWep loading model. The loading surface's distance from the detonation source and the equal amount of TNT for explosive must be provided for ConWep. ConWep loading model calculates the maximum overpressure, the arrival time, the duration of the positive phase, and the exponential decay coefficient for both incident pressure and reflected waves that originate as a result of the explosion of ALMs or IEDs. According to Eq.6, incident pressure on a surface can be expressed as a function of time, the angle between the surface normal, and the vector defined by surface and source.

$$P(t) = P_{incident}(t)\left[1+\cos\theta-2(\cos\theta)^2\right] + P_{reflect}(t)(\cos\theta)^2 \quad (6)$$

for $\cos\theta \geq 0$,

$$P(t) = P_{incident}(t) \text{ for } \cos\theta < 0 \quad (7)$$

The simulation was run for 4 milliseconds with merged nodes that correspond to the situation when an armor steel plate is attached to the undercarriage or side of the anti-landmine vehicle.

4. RESULTS AND DISCUSSION

The results of explicit dynamic analysis of all three FEM models were compared in order to determine which geometry is the best to use as anti-mining protection. All models were tested with a simulated TNT weight of 8, 10, and 12 kg.

The parameters chosen to compare the obtained results of each model individually are the maximal value of plastic strain and the maximal value of the vertical displacement of the central node on the protective plate, which is located on the longitudinal plane of symmetry in the direction perpendicular to the protective plate.

4.1 Model 1

Fig. 4-6 show the field of distribution of the plastic strain on the protective plate for model 1 in several views. For this case, the TNT mass of 8 kg was approximated. The maximum value of the plastic strain is 0.051.

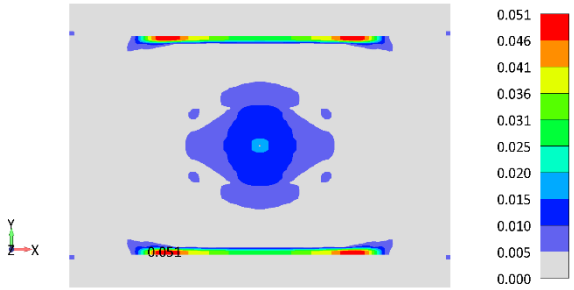

Fig.4. Plate Top/Bot effective plastic strain - model 1 Top view/TNT 8 kg

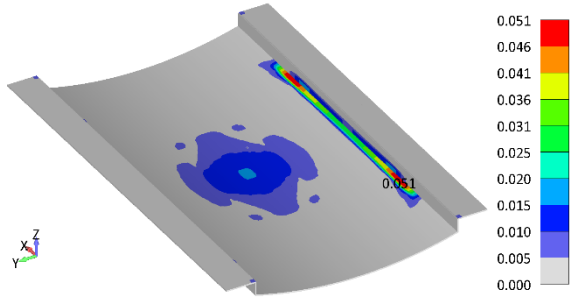

Fig.5. Plate Top/Bot effective plastic strain - model 1 Isometric view/TNT 8 kg

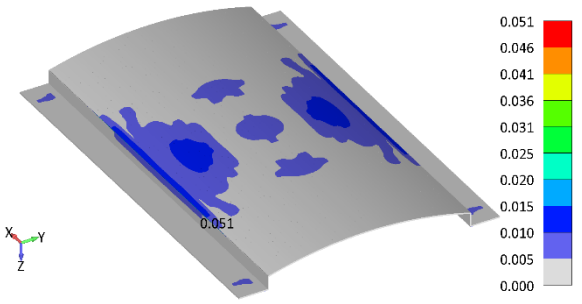

Fig.6. Plate Top/Bot effective plastic strain - model 1 Bottom view/TNT 8 kg

Fig. 7-9 show the field of distribution of the plastic strain on the protective plate for model 1 in several views. For this case, the TNT mass of 10 kg was approximated. The maximum value of the plastic strain is 0.055.

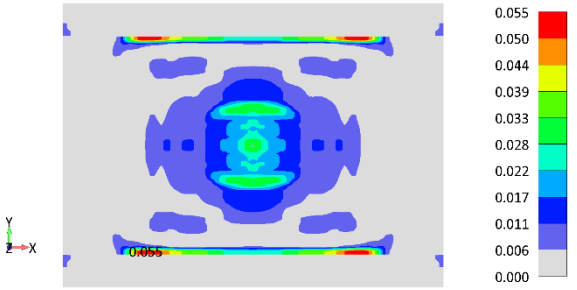

Fig.7. Plate Top/Bot effective plastic strain - model 1 Top view/TNT 10 kg

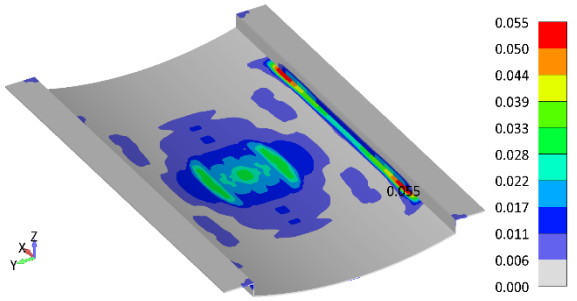

Fig.8. Plate Top/Bot effective plastic strain - model 1 Isometric view/10 kg

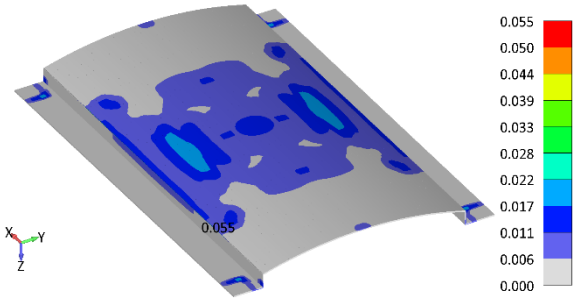

Fig.9. Plate Top/Bot effective plastic strain - model 1 Bottom view/TNT 10 kg

Fig. 10-12 show the field of distribution of the plastic strain on the protective plate for model 1 in several views. For this case, the TNT mass of 12 kg was approximated. The maximum value of the plastic strain is 0.055.

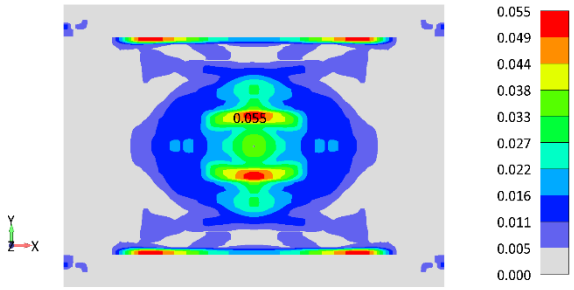

Fig.10. Plate Top/Bot effective plastic strain - model 1 Top view/TNT 12 kg

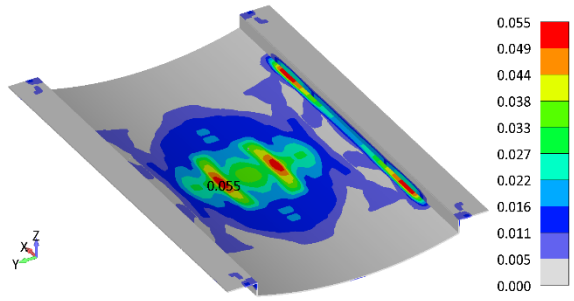

Fig.11. Plate Top/Bot effective plastic strain - model 1 Isometric view/TNT 12 kg

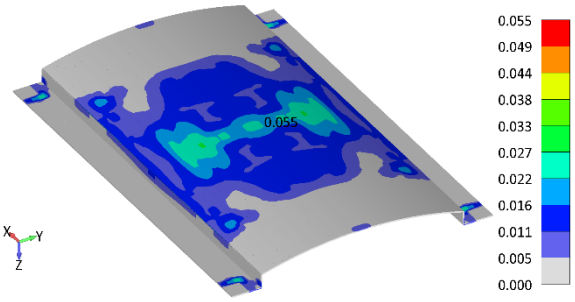

Fig.12. Plate Top/Bot effective plastic strain - model 1 Bottom view/TNT 12 kg

Maximal values of the plastic strain in dependence of time in elements were chosen as parameters to represent the results. For comparative analysis the elements in which the maximal values of plastic strain were obtained at the end of the analysis for load cases of 8 kg, 10 kg, and 12 kg of TNT for model 1 are shown in the diagram within Fig. 13. In Fig. 13, it can also be seen that the mass of TNT of 12 kg generates a higher pressure of the impact wave, which leads to an earlier start of plastic deformation on the protective plate for this type of geometry.

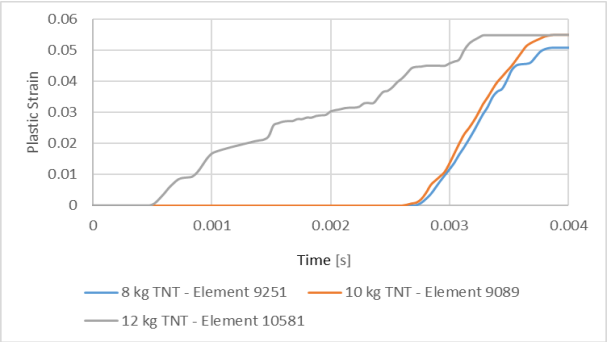

Fig.13. Maximal value of the plastic strain – model 1

The parameter chosen to compare the results obtained by each model individually is the vertical displacement of the central node on the protective plate located on the longitudinal plane symmetry in the direction perpendicular to the protective plate. The values of the vertical displacement for model 1 are shown in the diagram within Fig. 14.

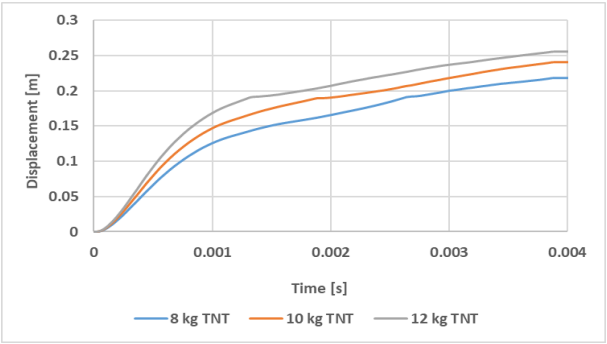

Fig.14. Vertical displacement of the central node at the longitudinal plane of symmetry of the protective plate – model 1

4.2 Model 2

Fig. 15-17 show the field of distribution of the plastic strain on the protective plate for model 2 in several views. For this case, the TNT mass of 8 kg was approximated. The maximum value of the plastic strain is 0.101.

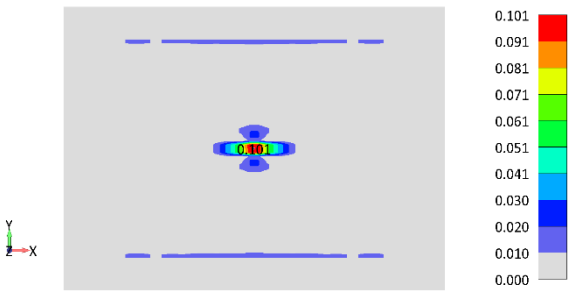

Fig.15. Plate Top/Bot effective plastic strain - model 2 Top view/TNT 8 kg

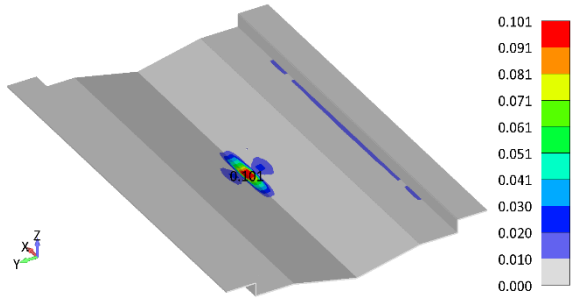

Fig.16. Plate Top/Bot effective plastic strain - model 2 Isometric view/TNT 8 kg

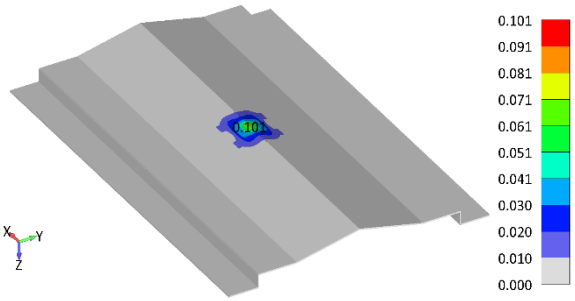

Fig.17. Plate Top/Bot effective plastic strain - model 2 Bottom view/TNT 8 kg

Fig. 18-20 show the field of distribution of the plastic strain on the protective plate for model 2 in several views. For this case, the TNT mass of 10 kg was approximated. The maximum value of the plastic strain is 0.117.

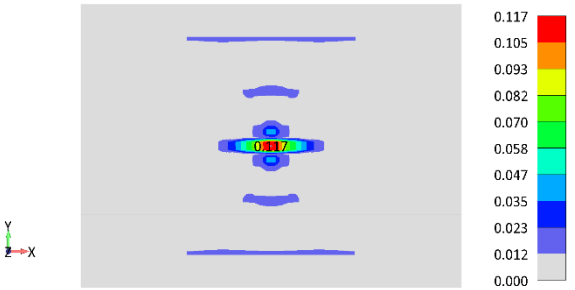

Fig.18. Plate Top/Bot effective plastic strain - model 2 Top view/TNT 10 kg

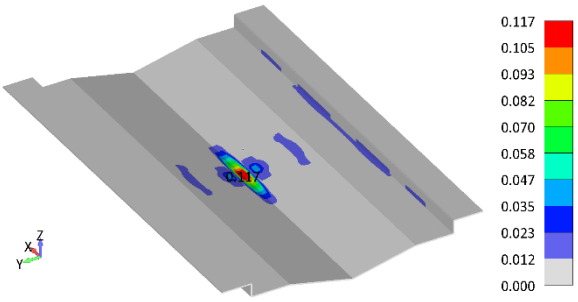

Fig.19. Plate Top/Bot effective plastic strain - model 2 Isometric view/TNT 10 kg

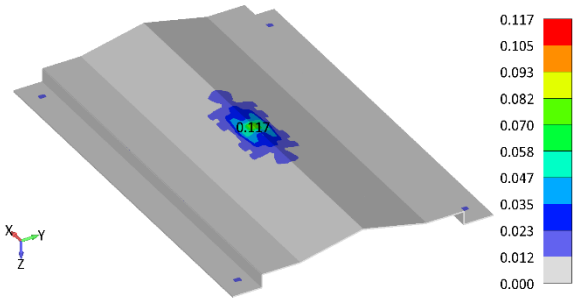

Fig.20. Plate Top/Bot effective plastic strain - model 2 Bottom view/TNT 10 kg

Fig. 21-23 show the field of distribution of the plastic strain on the protective plate for model 2 in several views. For this case, the TNT mass of 12 kg was approximated. The maximum value of the plastic strain is 0.117.

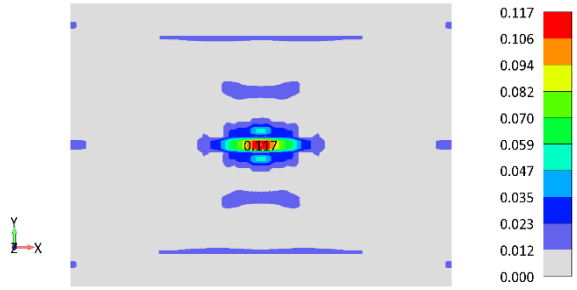

Fig.21. Plate Top/Bot effective plastic strain - model 2 Top view/TNT 12 kg

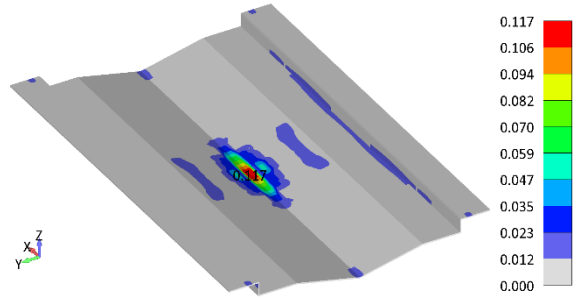

Fig.22. Plate Top/Bot effective plastic strain - model 2 Isometric view/TNT 12 kg

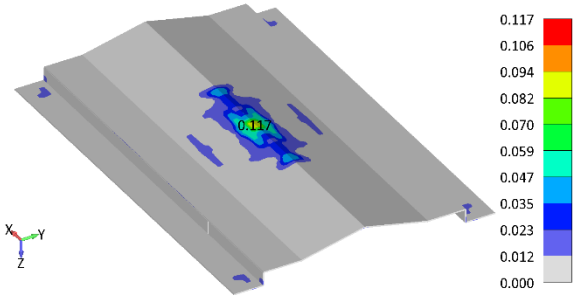

Fig.23. Plate Top/Bot effective plastic strain - model 2 Bottom view/TNT 12 kg

Maximal values of the plastic strain in dependence of time in elements were chosen as parameters to represent the results. For comparative analysis the elements in which the maximal values of plastic strain were obtained at the end of the analysis for load cases of 8 kg, 10 kg, and 12 kg of TNT for model 2 are shown in the diagram within Fig. 24.

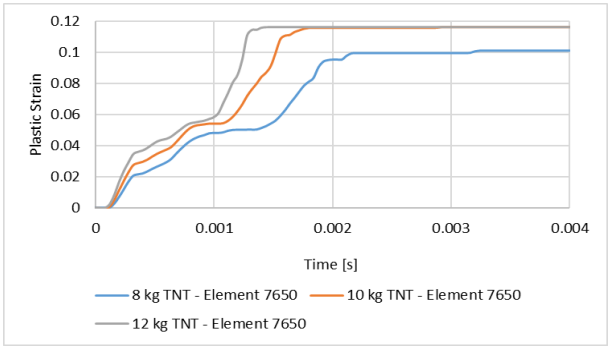

Fig.24. Maximal value of the plastic strain – model 2

The parameter chosen to compare the results obtained by each model individually is the vertical displacement of the central node on the protective plate located on the longitudinal plane symmetry in the direction perpendicular to the protective plate. The values of the vertical displacement for model 2 are shown in the diagram within Fig. 25.

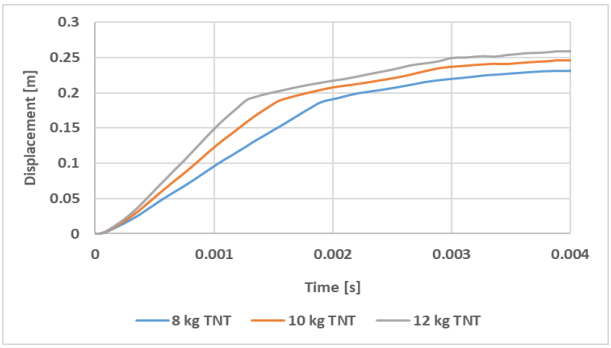

Fig.25. Vertical displacement of the central node at the longitudinal plane of symmetry of the protective plate – model 2

4.3 Model 3

Fig. 26-28 show the field of distribution of the plastic strain on the protective plate for model 3 in several views. For this case, the TNT mass of 8 kg was approximated. The maximum value of the plastic strain is 0.026.

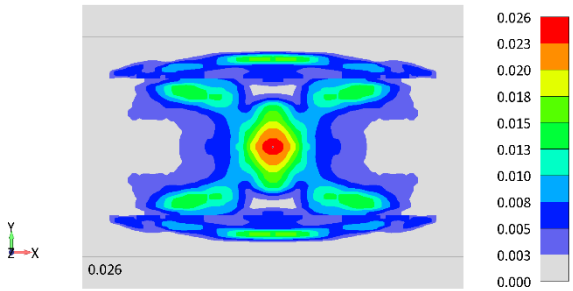

Fig.26. Plate Top/Bot effective plastic strain - model 3 Top view/TNT 8 kg

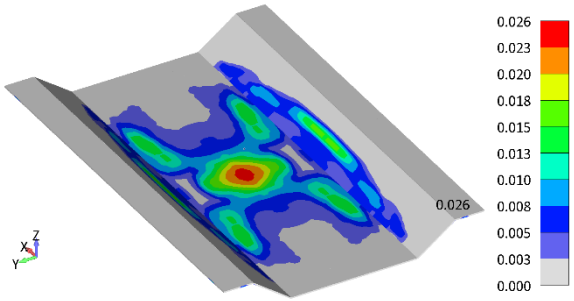

Fig.27. Plate Top/Bot effective plastic strain - model 3 Isometric view/TNT 8 kg

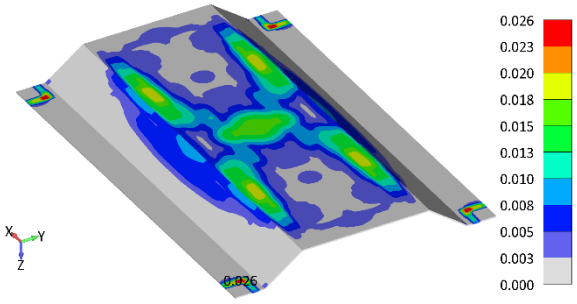

Fig.28. Plate Top/Bot effective plastic strain - model 3 Bottom view/TNT 8 kg

Fig. 29-31 show the field of distribution of the plastic strain on the protective plate for model 3 in several views. For this case, the TNT mass of 10 kg was approximated. The maximum value of the plastic strain is 0.043.

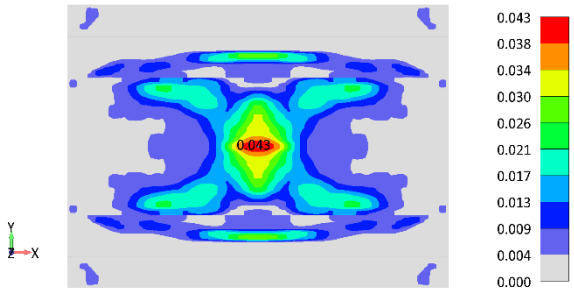

Fig.29. Plate Top/Bot effective plastic strain - model 3 Top view/TNT 10 kg

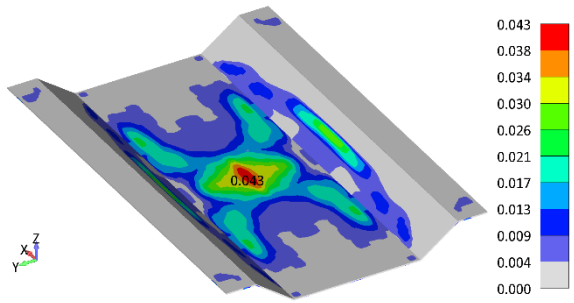

Fig.30. Plate Top/Bot effective plastic strain - model 3 Isometric view/TNT 10 kg

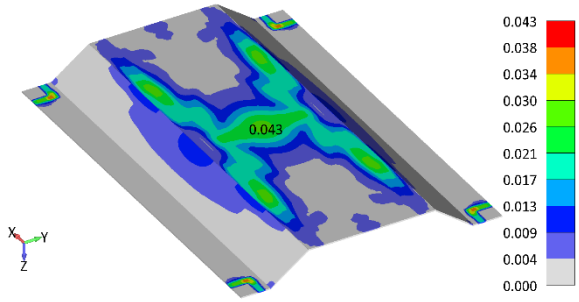

Fig.31. Plate Top/Bot effective plastic strain - model 3 Bottom view/TNT10 kg

Fig. 32-34 show the field of distribution of the plastic strain on the protective plate for model 3 in several views. For this case, the TNT mass of 12 kg was approximated. The maximum value of the plastic strain is 0.072.

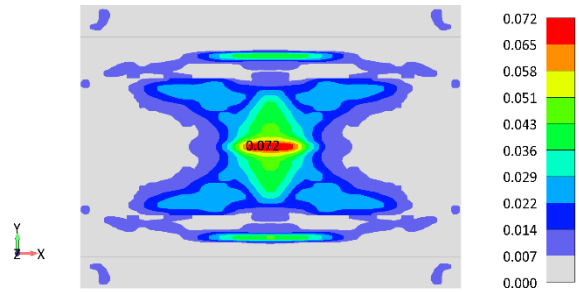

Fig.32. Plate Top/Bot effective plastic strain - model 3 Top view/TNT 12 kg

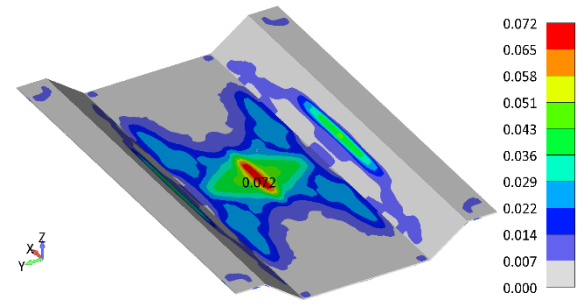

Fig.33. Plate Top/Bot effective plastic strain - model 3 Isometric view/TNT 12 kg

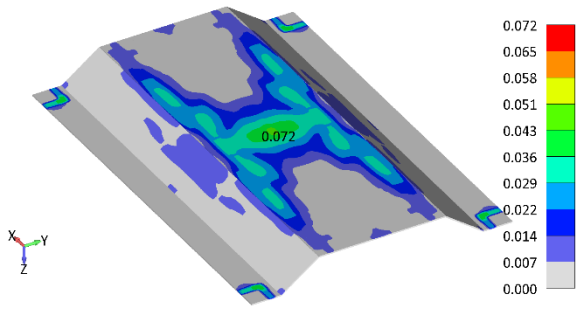

Fig.34. Plate Top/Bot effective plastic strain - model 3 Bottom view/TNT 12 kg

Maximal values of the plastic strain in dependence of time in elements were chosen as parameters to represent the results. For comparative analysis the elements in which the

maximal values of plastic strain were obtained at the end of the analysis for load cases of 8 kg, 10 kg, and 12 kg of TNT for model 3 are shown in the diagram within Fig. 35. In Fig. 35, it can also be seen that the mass of TNT of 10 and 12 kg generates a higher pressure of the impact wave, which leads to an earlier start of plastic deformation on the protective plates for this type of geometry.

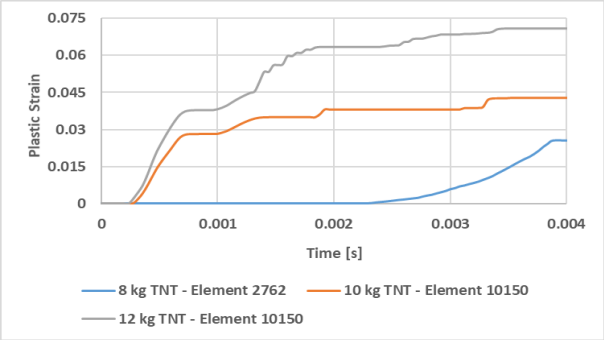

Fig. 35. Maximal value of the plastic strain – model 3

The parameter chosen to compare the results obtained by each model individually is the vertical displacement of the central node on the protective plate located on the longitudinal plane symmetry in the direction perpendicular to the protective plate. The values of the vertical displacement for model 3 are shown in the diagram within Fig. 36.

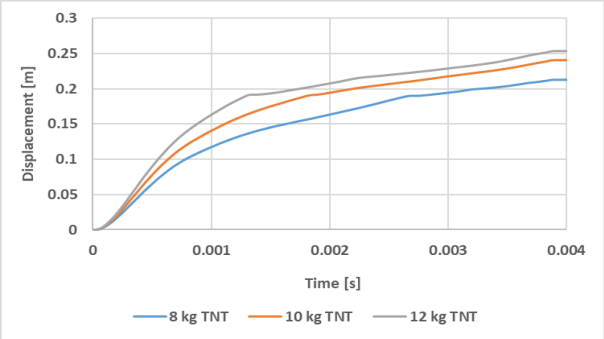

Fig.36. Vertical displacement of the central node at the longitudinal plane of symmetry of the protective plate – model 3

5. CONCLUSION

Based on the obtained results it can be concluded:

- In models 1 and 2, with the increase of explosive mass, there is an increase in the value of plastic strain, with the fact that in models with 10 kg and 12 kg of explosive mass this value is almost the same.
- In models 1 and 2, when the mass of the explosive is 12 kg, it can be concluded that the plastic strain starts earlier, due to the higher pressure of the impact wave because of the higher mass of the explosive.
- In model 3, with increasing explosive mass, the values of the plastic strain increase.
- For the load case of 8 kg of TNT mass, in all three models, it can be concluded that the plastic strain begins in model 2 between 0 and 0.001 s of the analysis, while in models 1 and 3 the plastic strain begins between 0.002 and 0.003 s of the analysis, and the plastic strain has the smallest value in model 3.
- For the load case of 10 kg of TNT, in all three models, it can be concluded that the plastic strain begins in models 2 and 3, between 0 and 0.001 s of the analysis, while in model 1 the plastic strain begins between 0.002 and 0.003 s of the analysis, and the plastic strain has the smallest value in model 3.
- For the load case of 12 kg of TNT, in all three models, it can be concluded that the plastic strain in the three models begins between 0 and 0.001 s of the analysis, and the plastic strain has the smallest value in model 1.
- For all three load cases (8 kg, 10 kg, and 12kg of TNT), model 2 has the highest plastic strain.
- In all models, with increasing explosive mass, the vertical displacement of the central node on the protective plate increases.
- The largest vertical displacement of the central node on the protective plate, i.e. the lowest stiffness has a protective plate in model 2.
- The smallest vertical displacement of the central node on the protective plate, i.e. the highest stiffness has a protective plate in model 3.
- Analyzing all three models, it is concluded that the lowest values of plastic strain (except for the case when the mass of the explosive is 12 kg) and the smallest vertical displacement of the central node on the protective plate have model 3. For these reasons, it is recommended that model 3 be used as anti-landmine protection.
- Designing anti-mining protection should be an integral part of the process of designing a complete vehicle because in this way a more favorable configuration of protection can be achieved.

- The development of ALM protection on already built and operated vehicles, which do not have ALM protection, is hampered by the requirements of clearance, the present geometric restrictions, and the existing performance of vehicles that must not be endangered.

Acknowledgements

This research is partly supported by the Ministry of Education and Science, Republic of Serbia, Grant 451-03-68/2022-14/ 200378, and Grant TR32036.

REFERENCES

[1] M.R. Sunil Kumar, E. Schmidova, Deformation Response of Dual Phase Steel in Static and Dynamic Conditions. *Applied Engineering Letters*, 4(2), 2019: 41-47. https://doi.org/10.18485/aeletters.2019.4.2.1

[2] A. Belhocine, O.I. Abdullah, Finite element analysis (FEA) of frictional contact phenomenon on vehicle braking system. *Mechanics Based Design of Structures and Machines*, 5(9), 2022: 2961-2996. https://doi.org/10.1080/15397734.2020.1787843

[3] S. Mahajan, R. Muralidharan, Simulation of an Armoured Vehicle for Blast Loading. *Defence Science Journal*, 67(4), 2017: 449. https://doi.org/10.14429/dsj.67.11430

[4] Kartikeya, S. Prasad, N. Bhatnagar, Finite Element Simulation of Armor Steel used for Blast Protection. *Procedia Structural Integrity*, 14, 2019: 514-520. https://doi.org/10.1016/j.prostr.2019.05.066

[5] J. Trajkovski, J. Perenda, R. Kunc, Blast response of Light Armoured Vehicles (LAVs) with flat and V-hull floor. *Thin-Walled Structures*, 131, 2018: 238-244. https://doi.org/10.1016/j.tws.2018.06.040

[6] M. Cong, Y. Zhou, M. Zhang, X. Sun, C. Chen, C. Ji, Design and optimization of multi-V hulls of light armoured vehicles under blast loads. *Thin-Walled Structures*, 168, 2021: 108311. https://doi.org/10.1016/j.tws.2021.108311

[7] A. Markose, C.L. Rao, Mechanical response of V shaped plates under blast loading. *Thin-Walled Structures*, 115, 2017: 12–20. https://doi.org/10.1016/j.tws.2017.02.002

[8] M. Ivančo, R. Erdélyiová, L. Figuli, Simulation of detonation and blast waves propagation. *Transportation Research Procedia*, 40, 2019: 1356–1363. https://doi.org/10.1016/j.trpro.2019.07.188

[9] Ramasamy, A. Hill, A. Hepper, A. Bull, J. Clasper, Blast Mines: Physics, Injury Mechanisms and Vehicle Protection. *Journal of the Royal Army Medical Corps*, 155, 2009: 258-264. https://doi.org/10.1136/jramc-155-04-06

[10] J.W. Denny, A.S. Dickinson, G.S. Langdon, Defining blast loading 'zones of relevance' for primary blast injury research: A consensus of injury criteria for idealised explosive scenarios. *Medical Engineering & Physics*, 93, 2021: 83-92. https://doi.org/10.1016/j.medengphy.2021.05.014

[11] NATO, *„AEP-55 Vol2 Procedures for Evaluating the Protection Level of Armoured Vehicles – Mine Threat*, "NATO Standardization Agency, 2014.

[12] C.H. Choi, M. Callaghan, B. Dixon, Blast Performance of Four Armour Materials Executive Summary. *Land Division DSTO Defence Science and Technology Organisation, Victoria 3207 Australia*. 2013.

[13] T. Fu, M. Zhang, Q. Zheng, D. Zhou, X. Sun, X. Wang, Scaling the response of armor steel subjected to blast loading. *International Journal of Impact Engineering*, 153, 2021: 103863. https://doi.org/10.1016/j.ijimpeng.2021.103863

[14] Response of Armour Steel Plates to localised Air Blast Load – A Dimensional Analysis, *IJM*. 11, 2017.

[15] E. Palta, M. Gutowski, H. Fang, A numerical study of steel and hybrid armor plates under ballistic impacts. *International Journal of Solids and Structures*. 136-137, 2018: 279-294. https://doi.org/ 10.1016/j.ijsolstr.2017.12.021

[16] M. French, A. Wright, Developing mine blast resistance for composite based military vehicles. *In: Blast Protection of Civil Infrastructures and Vehicles Using Composites. Elsevier*. 2010: 244-268. https://doi.org/10.1533/9781845698034.2.244

[17] R. Aguiar, O.E. Petel, R.E. Miller, Effect of a Halloysite-polyurethane nanocomposite interlayer on the ballistic performance of laminate transparent armour. *Composites Part C: Open Access*, 7, 2022: 100231. https://doi.org/10.1016/j.jcomc.2022.100231

[18] P. Zhang, D. Mo, X. Ge, H. Wang, C. Zhang, Y. Cheng, J. Liu, Experimental investigation into the synergetic damage of foam-filled and unfilled corrugated core hybrid sandwich panels under combined blast and fragment loading. *Composite Structures*. 299, 2022: 116089. https://doi.org/10.1016/j.compstruct.2022.116089

[19] Z. Yi, A.K. Agrawal, M. Ettouney, S. Alampalli, Finite Element Simulation of Blast Loads on Reinforced Concrete Structures using LS-DYNA. *In: New Horizons and Better Practices. American Society of Civil Engineers, Long Beach, California, United States*. 2007: 1–10. https://doi.org/10.1061/40946(248)3

[20] A. Dišić, Development of methodology and devices for dynamic testing of materials and welded joints with application in numerical calculations of structures at high deformation rates – PhD Thesis, *Faculty of Engineering University of Kragujevac*, *Serbia*, 2018.

[21] D. Varecha, O. Bokůvka, L. Trško, M. Vicen, R. Nikolić, Influence of Ultrasonic Impact Treatment on the Fatigue Safety Coefficients of Welded Joints of the Strenx 700MC Steel. *Applied Engineering Letters*, 5 (3), 2020: 75–79. https://doi.org/10.18485/aeletters.2020.5.3.1

[22] Femap, Finite Element Modeling and PostProcessing Application FEMAP v2021.2, Siemens, 2021.

[23] LS-DYNA, LS-PrePost-4.5-A New Post Processor for Use LSDYNA, California: Livermore, 2014.

[24] T.P. Slavik, A coupling of empirical explosive blast loads to ALE air domains in LS-DYNA®. *IOP Conference Series: Materials Science and Engineering*, 10, 2010: 012146. https://doi.org/10.1088/1757-899X/10/1/012146

[25] S.M. Kalawadwala, S. Rigby, Setting up Load Blast Enhanced in LS-DYNA. 2016. https://doi.org/10.13140/RG.2.1.1426.8402